Phosphorus deposition on a three-way catalyst under accelerated ageing conditions

Benjamin, S.F. , Brogan, M. , Collin, T. , Disdale, W. , Roberts, C.A. and Wei, J.

Original citation & hyperlink:
Benjamin, S.F. , Brogan, M. , Collin, T. , Disdale, W. , Roberts, C.A. and Wei, J. (2012) Phosphorus deposition on a three-way catalyst under accelerated ageing conditions. Proceedings of the Institution of Mechanical Engineers, Part D: Journal of Automobile Engineering, volume 226 (2): 247-259.
http://dx.doi.org/10.1177/0954407011414480

Phosphorous deposition on a three way catalyst under accelerated ageing conditions

S. F. Benjamin[a], M. Brogan[b], T. Collin[c], W. Disdale[a], C. A. Roberts[a]*, J. Wei[d]

a Automotive Engineering Applied Research Group, Coventry University, UK

b Ford Motor Company, Dunton Technical Centre, Laindon, UK

c BASF Catalysts, Hannover, Germany

d BASF Catalysts, Iselin, New Jersey, USA

* Corresponding author

Abstract

Degradation of catalyst performance with time is described as ageing. There are two significant ageing mechanisms, poisoning and sintering. Experimental data on ageing has been obtained on an engine test bed using a specially designed catalyst core holder that has subjected catalyst samples to different accelerated ageing regimes and durations. The ageing regimes were low temperature dosed (mainly poisoning), high temperature (mainly sintering) and high temperature dosed (both sintering and poisoning). The experiments provided a series of samples from which the spatial and time dependency of the poisoning has been found. Portions of the samples were subjected to XRF analysis following ageing. A combined model of poisoning and sintering was developed and incorporated into a CFD model. This combined model can predict the level of deactivation as a function of length along the catalyst and as a function of time. Agreement between measured poison accumulation and predictions was achieved by tuning of the sintering parameter.

Keywords

Catalyst, poisoning, sintering, ageing, CFD model

1.0 Introduction

Automotive exhaust catalyst degradation by ageing prevents the out-of-factory emissions levels being maintained throughout the converter's life. Ever more stringent emissions restrictions being imposed by governments in Europe and the US mean that deterioration in catalyst performance with time cannot be tolerated.

The old solution of oversized catalysts is now unacceptable as this adds to costs and occupies valuable space in smaller vehicles.

This study focuses on the standard three-way catalyst for gasoline engines that converts CO, hydrocarbons and NOx. There are several deterioration or ageing mechanisms that can affect its performance **[1]**. These mechanisms lessen the active surface area of precious metal catalyst available to promote the species conversion reactions, but they do it in several different ways. Poisoning is a mainly chemical effect whereby atoms of elements such as Phosphorous (P), Sulphur (S), Zinc (Zn) or other poisons occupy reaction sites on the precious metal catalyst particles so that they are unavailable for promotion of the required conversion reactions. The behaviour of phosphorous compounds suggests that phosphorous can continue to accumulate even after a site is deactivated. The origin of the poison atoms is often the engine oil, or from combustion of additives in the oil or fuel, particularly the anti-wear agent zinc dithiophosphate, ZDP, **[2]** or ZDDP, zinc dialkyldithiophosphate. Blocking of pores in the catalyst washcoat by poisons can have a similar deactivating effect, making many active sites inaccessible if a significant pore volume is blocked. It has been known for many years **[3]** that there is a tendency for phosphorous compounds to sinter and form a glassy layer, which can have this effect. Sintering, on the other hand, is a mainly mechanical or thermal effect whereby the small precious metal particles clump together to form larger masses of precious metal that have significantly smaller surface area to mass ratio. Sintering tends to occur at higher temperatures than poisoning. At excessively high temperatures fusing of the ceramic substrate material can also occur and this can destroy the pores and lessen the active surface area. This can be described as substrate sintering, but it is the sintering of the precious metal particles that is considered in this paper.

There have been numerous attempts to investigate and model catalyst deactivation and ageing over the years. Accelerated ageing on an engine test bed was investigated by Gonzalez-Velasco et al. **[4]** in 2000 and more recently Nagashima et al. **[5]** have proposed a sintering model. They concluded that catalytic performance is not a simple function of surface area of precious metal particles and suggest that the activation energy for CO and HC oxidation reactions changes after ageing.

An experimental investigation of rapid or accelerated catalyst ageing on an engine test bed has been carried out. The aim was to reveal the spatial and time dependency of accelerated ageing. Using an engine test bed and a

demountable catalyst core holder, a number of cores were subjected to different ageing regimes. This provided a selection of time-aged cores that could be subjected to physical analyses. Of particular interest in this study has been the interaction between the two mechanisms, poisoning and sintering, and their relative influence on deactivation at different times and catalyst locations. A model to describe simultaneous poisoning and sintering has been developed in this study. This was based on the long established poisoning model of Oh et al. **[6]** and the more recent sintering model of Matsunaga et al. **[7]**. The combined model was introduced into a CFD model based on the porous medium approach. This combined model was able to make predictions about the degree of deactivation as a function of time and of location along the length of the catalyst. Previous work has shown that poisons tend to accumulate locally near the entrance to the monolith **[8]** and this has been confirmed in this new study. The experimental studies of accelerated ageing on an engine test bed and the development of the combined poisoning and sintering model are both described in this paper. The model predictions are compared with XRF measurements of phosphorous in the samples.

2.0 Experimental studies

The experimental arrangement on the engine test bed is shown in Fig. 1. The engine was a Ford 1.6 litre sigma gasoline engine running with an approximately stoichiometric air/fuel ratio, very slightly rich, λ=0.993. The engine was operating at a steady state condition in every case with its temperature controlled. The temperature was maintained at the catalyst inlet via running speed and engine load adjustments. The demountable catalyst can that contained the catalyst core holder can be seen circled in black in Figure 1. The detail of the core holder can be seen in Figure 2. Each of the seven cores held by the can core was 25.4 mm in diameter and 127 mm in length. The catalyst cores had typical three-way conversion characteristics and were provided by BASF, formerly Engelhard™. The catalyst was a blend of Pd and Rh in approximately equal parts, and Ce and Zr were also present. The cores were calcinated for one hour in the temperature range 723 to 823 K so that they were pre-conditioned. The core holder, loaded with conditioned cores, was inserted into the can and ageing commenced on the test bed. At strategic intervals, the cores were extracted and replaced, so that the samples were exposed to known regimes and the rate of deactivation and physical change could be assessed. The core holder was filled with cores at all times so that the flow pattern was consistent.

Figure 3 shows the core numbering scheme. TC indicates a core fitted with thermocouples and M indicates the middle core. The TC core had two thermocouples inserted into the side of the core, 25.4 mm from the inlet and 25.4 mm from the exit. There were also thermocouples pre and post the catalyst cores that monitored the gas temperatures, as can be seen in Fig. 1.

The ageing regimes are shown in Table 1. Each regime generated 10 variously aged cores. The regimes were designed to promote mainly poisoning by dosing at low temperature (LTD), mainly sintering by operating at high temperature without dosing (HT) and both poisoning and sintering by operating at high temperature with dosing (HTD). The dosing agent was ZDDP, which is a source of phosphorous. The ZDDP was added to the forecourt grade petrol in concentrations ≤ 150 ppm. The ZDDP was added to the fuel because leakage from the oil, the normal migration route, would neither have allowed control of the dose, nor been fast enough for a rapid ageing test. The dosing rate was adjusted so that the total dose was similar after 40 hours in the HTD case and after 100 hours in the LTD case; the values are given in Table 2. Thus 8 hours in the HTD regime was approximately equivalent to 20 hours in the LTD regime in terms of total phosphorous exposure. The P mass fraction in table 2 is also expressed as an equivalent mass fraction of H_3PO_4, assumed to be the poison precursor, by multiplying by the ratio of the molecular masses (97.97/30.97). The poison precursor mass fraction, rather than the phosphorous mass fraction, is required for input to the CFD model.

Each regime was interrupted four times for a core change. This meant a core change every 8 hours for the HT and HTD cases and every 20 hours for the LTD case. Table 3 shows the details of the cores that were subsequently analysed and that are the basis for the information presented in this paper. The middle core had experienced a total of 180 hours of deactivation, 100 hours of mainly poisoning, followed by 40 hours of sintering, and finally 40 hours of both mechanisms.

Each core identified in Table 3 was analysed for chemical composition. The 127 mm length cores were cut into four equal length sections, referred to as segments in this paper. The segments were theoretically 31.75 mm in length, but in practice there was a small loss, less than 2.5 % of length, attributable to the cutting procedure. All four core segments were submitted for chemical analysis using XRF. The segments were crushed for the analysis so that the crushed sample contained the substrate, washcoat, precious metal and contaminants.

3.0 Development of combined poisoning and sintering model

An ageing model was developed by combining a pre-existing poisoning model **[6]** with a pre-existing sintering model **[7, 8]** in order to aid interpretation of measurements from the experimental programme.

3.1 Poisoning model

In the catalyst washcoat layer, an irreversible reaction occurs between the poison precursor and the active catalyst site. This reaction is assumed independent of temperature **[6]**. The specific rate for the poisoning of the catalyst was defined, using the original units as described by Oh and Cavendish **[6]**, by the expression

$$C_{W\infty}\frac{d\theta}{dt} = -k_P\,(1 - \theta_w)\;C_{SP} = -k_P\;\theta\;C_{SP} \qquad (1)$$

θw is the fraction of active sites that are deactivated by the deposited poison and θ is the fraction of sites that are free and active. The rate [$C_{W\infty}\,d\theta/dt$] is expressed in mol P/s/cm^2 BET surface area, but C_{SP} is the molar concentration of poison precursor, H_3PO_4. The original value for k_P used by Oh and Cavendish **[6]** was 0.1 cm/s.

Revising eq. (1) to modify the units and rearranging gives eq. (2)

$$\frac{d\theta}{dt} = -K_P\;\theta\;C_{WP}\;/\;C_{Winf} = -X\;\theta \qquad (2)$$

where K_P is the rate constant [0.001 (30.97/97.97) $\rho_g\,A_{BET}$]. The poisoning rate [$C_{Winf}\,(d\theta/dt)$] is expressed in kg P/s/m^3 reactor, where C_{Winf} is the saturation concentration of phosphorous. The quantity C_{WP} is mass fraction of H_3PO_4 (M 97.97), rather than P (M 30.97); it is generally a function of time and position along the catalyst. At the inlet to the catalyst, however, eq. (2) has an analytical solution eq. (3) that describes the decay of the active surface area at the catalyst inlet with time as a result of poisoning.

$$\theta = \exp[-X\,t] \qquad (3)$$

3.2 Sintering model

Matsunaga et al. [7] considered the role of catalyst particle mean diameter on performance. They derived an expression for the rate of particle diameter enlargement, i.e. sintering.

$$\frac{dD}{dt} = \frac{A}{D} [O_2]^{2/3} \exp(-E/RT) \quad (4)$$

The fraction of the active precious metal surface area available for catalysis is 1 when the catalyst is fresh and less than 1 as the catalyst ages. Hence for sintering, the fraction may be represented as the particle diameter ratio, eq. (5). This relationship is based on the assumption that the active surface is the outer surface of spherical particles of precious metal. The particles enlarge in size but decrease in number as the sintering process progresses, but the total mass and volume of precious metal remain the same. This assumption is different from the assumption that the catalyst particles form a thin "carpet" or active layer spread over the surface of the pores in the washcoat, which provides poorer surface coverage as the particles sinter together.

$$\theta = D_O/D \quad (5)$$

Differentiating eq. (5) and multiplying by eq. (4) gives eq. (6).

$$\frac{d\theta}{dt} = -A \frac{\theta^3}{D_O^2} [O_2]^{2/3} \exp(-E/RT) = -W \theta^3 \quad (6)$$

A term was added to eq. (4) in **[8]** to allow for the suppression of sintering by poisoning, but this term is excluded here. The term is excluded because mutual inhibition between poisoning and sintering is accounted for by combining eqs. (2) and (6), which is discussed in section 3.3 below.

Equation (6) has an analytical solution eq. (7) that describes the decline of active surface area with time at the catalyst monolith inlet as a result of particle sintering.

$$\theta = 1/\sqrt{[2Wt + 1]} \quad (7)$$

This model can predict very small theta values that correspond to non-physical values for *D*. Calculation can reveal a realistic minimum value for theta. For example, if D_O is 5.0E-10 m, and a litre catalyst supports 3 grams of precious metal, then if, hypothetically, the catalyst on one core in the experiment described here was sintered to a single particle, it would have a diameter of about 2.5 mm. This corresponds to a minimum possible value for theta of about 2.0E-07. Nagashima et al. **[5]** observed precious metal surface area reductions down to only about one hundredth of the fresh value in ageing experiments. In the real case therefore, theta would not be

expected to fall much below 0.01, possibly down to 1.0 E-04 based on reasonable estimates of maximum sintered particle size. There has been an attempt **[9]** to modify this model to account for this anomaly, but the simpler original form of the model is applied here.

3.3 Combined poisoning and sintering model

The combined model is developed by adding the rates of poisoning and sintering to give eq. (8). This couples the poisoning and sintering mechanisms.

$$\frac{d\theta}{dt} = -W\,\theta^3 - X\,\theta \qquad (8)$$

In eq. (8) W is (A $[O_2]^{2/3}$ / D_O^2) exp (–*E*/R*T*) and X is $K_P\, C_{WP} / C_{Winf}$

Equation (8) can be solved analytically by partial fractions and substitution to give eq. (9), which applies at the catalyst monolith inlet

$$\theta = 1/\sqrt{[\exp(2Xt) + (W/X)(\exp(2Xt)-1))]} \qquad (9)$$

Values for the parameters used in the deactivation model are given in Table 4, with C_{WP} and $[O_2]$ being inlet gas phase values. The model is sensitive to both C_{WP} and $[O_2]$ values, so the deactivation will be less downstream from the inlet because of the effects of mass transfer along the length of the sample. Also, gas phase concentrations are generally lower in the pores of the washcoat than in the flowing gas phase so C_{WP} and $[O_2]$ can be corrected to allow for this when applying eq. (9) to obtain analytical predictions. The factors given in Table 4 allow for phosphorous deposition in the engine and supply pipework and these are discussed later. The parameter K_P listed in Table 4 was discussed in Section 3.1. The value of A in the sintering model has been selected to ensure that sintering was sufficiently slow to enable P to be adsorbed right through to the end of the middle core ageing; the model therefore predicts deactivation in all three cases, compatible with the observed accumulation of phosphorous, as discussed later. The A_{BET} and C_{Winf} values in Table 4 are based on the substrate washcoat loading. The initial diameter of the catalyst particle, D_O is 0.5 nm; this value is based on values from the literature, for example Cooper at al. **[10]**. It represents a metal particle with a diameter equivalent to about two atomic diameters.

The analytical solution eq. (9) predicts the plots shown in Fig. 4. These indicate deactivation at the inlet to the catalyst as a function of time. In Figure 4, the LTD100 case is dominated by poisoning, the HT40 case is exclusively sintering and the HTD40 case exhibits initially more sintering than poisoning, with all three cases performing as intended in the experimental methodology. Comparing the HT40 case with the HTD40 case in Figure 4 shows how the predicted sintering rate is influenced by poisoning.

The combined deactivation model was introduced into a CFD model using the porous medium approach **[11]** to model deactivation under experimental conditions. The solvers of a commercial CFD code are used to develop a model that could readily be applied to 3D cases where flow maldistribution can be significant. Five species were defined: CO, C_3H_6, NO, O_2 and a poison precursor in the gas stream, which is assumed to be phosphoric acid, H_3PO_4. The concentrations of species in the gas in the pores of the washcoat, i.e. in the solid phase, were solved for in the CFD model. The deactivation profile, θ as a function of both time and length along the substrate can then be found from the model. The deactivation parameter, θ, is used simultaneously to modify the conversion rates in the kinetic model that is applied during the ageing simulations. Only CO, C_3H_6, NO and O_2 are modelled in the kinetic model. The reaction chemistry used was the three-way scheme of Baba et al. **[8]**.

3.4 Governing equations for the CFD deactivation model

In the CFD model, the monolith axis is aligned in the z direction and there is no convection of species in the x and y directions in the porous medium. The equations below are presented in 1D form. For the gas phase species in the porous medium computational cell that represents the bulk monolith, the conservation equation eq. (10) below is solved. The term on the RHS of eq. (10) is the source term coded into a user subroutine of the CFD code.

$$\varepsilon \frac{\partial}{\partial t}[\rho_g C_{i\,g}] + \frac{\partial}{\partial z}[\rho_g U_S C_{i\,g}] = -K_{mi}\,\rho_g\,A_V\,[C_{i\,g} - C_{i\,sol}] \qquad (10)$$

For the solid phase species in the porous medium computational cell that represents the bulk monolith, eq. (11) below is solved. The source term on the RHS of eq. (11) is coded into the user subroutine.

$$\varepsilon \frac{\partial}{\partial t}[\rho_g C_{i\,sol}] = \{K_{mi}\,\rho_g\,A_V\,[C_{i\,g} - C_{i\,sol}] + M_i R_i\}[\varepsilon / V_w] \qquad (11)$$

In the deactivation model, when considering phosphoric acid as the poison precursor, $M_i R_i$ is the rate at which it is removed from the gas in the pores so that P can be stored or accumulate. This is the poisoning rate [C_{Winf} (dθ /dt)]. In the catalyst model, $M_i R_i$ is the rate of consumption of species by chemical reaction on the catalytic surface. The simulations included reaction chemistry, and the enthalpy of reactions is accounted for in establishing the temperature of the substrate. There is an additional equation, eq. (8), that must be solved in the deactivation model, in order to obtain a value for θ. This is re-expressed as eq. (12) in order that the CFD solver can be used to obtain θ.

$$\varepsilon \rho_g \frac{\partial \theta}{\partial t} = [- \mathrm{W}\ \theta^3 - \mathrm{X}\ \theta\ ]\ \varepsilon \rho_g \qquad (12)$$

The energy equation solved for the fluid cells is

$$\varepsilon \rho_g C_{Pg} \left[\frac{\partial T_g}{\partial t} + U_C \frac{\partial T_g}{\partial z} \right] - \varepsilon\ k_g \frac{\partial^2 T_g}{\partial z^2} = - h A_V [T_g - T_{sol}] \qquad (13)$$

The energy equation eq. (14) is solved in a separate block of solid cells to model the temperature of the solid walls in the monolithic catalyst or analogous porous medium.

$$(1 - \varepsilon)\ \rho_{sol} C_{Ps} \frac{\partial T_{sol}}{\partial t} - (1 - \varepsilon)\ k_{sol} \frac{\partial^2 T_{sol}}{\partial z^2} = - h A_V [T_{sol} - T_g] + \Delta H R_i \qquad (14)$$

4.0 Details of the computational simulations

The commercial CFD package Star-CD Version 3.26 was used throughout for the simulations. The catalyst substrate was modelled using the porous medium approach, as outlined above, where the scalar species are modelled in the porous medium cells but the heat conduction equation is solved in a separate block of solid cells that models the enthalpy in the monolith **[11, 12]**. The gas phase species were solved for in the porous medium cells and the pore phase species were also modelled in the porous medium cells but with the advection solver turned off. Allowance was made for the pore volume, see eq. (11) and reference **[12].** Heat transfer between porous medium cells and solid cells and mass transfer between the fluid and pore phases of the porous medium was managed within Star-CD by using user subroutines to apply appropriate heat and mass transfer coefficients. The simulations were carried out on one node of an Itanium 2 64-bit HP cluster under HP-UX.

4.1 Full ageing simulations with combined poisoning and sintering

The mesh for the full ageing simulations with both poisoning and sintering is shown in Figure 5. The model was 1D, but the method can be readily applied to 3D meshes if required. The mesh has 74 fluid cells plus 64 separate solid cells. Five fluid cells of length 2 mm comprise the short duct upstream of the porous medium and similarly downstream. The 64 cells in the porous medium spanned 127 mm so that each cell was of length just less than 2 mm. The simulations were run transient for 40 hours, 100 hours or 180 hours of real time, dependent upon which ageing regime was being modelled. Table 5 indicates the time step scheme for the 180 hour simulation, with progressively longer time steps used after the first minute of real time.

Each ageing simulation took a few hours of processing time. The total flow rate was found from the fuel flow rate in each case, and the mass flow rate per core was used in the simulation, from values in Table 2. The mass transfer of poison precursor, H_3PO_4, from the gas stream to the channel wall and into the washcoat was described by a mass transfer coefficient K_{bulk} , defined by eq. (15), where K_{air} is equal to Sh D_{air} / d_h .

$$1/K_{bulk} = 1/K_{air} + H/D_{WC} \qquad (15)$$

This resistance in series approximation for mass transfer coefficient is appropriate when using the analogous porous medium approach. Values for species diffusivity in washcoat were given in **[6]**. Depths at which P has been observed to be deposited in catalyst washcoats have been published **[13]**. A depth of 15 microns was used here for H. In the computational model, a value of 0.18 m/s for K_{bulk} was used for the LTD100 case and 0.305 m/s was used in the HTD40 case, with the temperature being significantly different in the two cases. These mass transfer coefficients were elevated in the computational cells up to 22 mm from the inlet in the high temperature and flow rate cases and up to 4 mm from the inlet in the low temperature and flow rate case to account for thermal and hydrodynamic boundary layer development on Sherwood number. Elevation factors were found by analogy with the behaviour of the Nusselt number in square channels **[14].**

5.0 Results

5.1 XRF chemical analysis results

Figure 6 shows how phosphorous, zinc and sulphur accumulate with time in the inlet segment of the catalyst cores. Sulphur levels are approximately constant with time in both the HTD40 test and the LTD100 test. The

middle core sample at 180 hours shows a slightly lower sulphur level, but this may be spurious. Levels of phosphorous and zinc are generally higher in the HTD 40 test than in the LTD100 test. Both species in both tests show progressive accumulation with time. More phosphorous is accumulated than zinc; phosphorous is assumed to be the main deactivating contaminant. The implications of this are that the deterioration in catalyst performance may be underestimated as the contamination of the active surface area by zinc and sulphur is neglected; the model focuses on the effect of phosphorous. The middle core at 180 hours shows the highest level of P. Thus it is clear that even after 100 hours of poisoning and a further 40 hours of high temperature sintering, the sample is capable of accumulating a further significant amount of phosphorous. This is further illustrated in Figure 7. The rate of poisoning in the first segment can be seen to be higher in the HTD40 experiment than in the LTD100 experiment. The middle core experiences no poisoning between 100 and 140 hours, but when it is finally exposed to the HTD40 regime between 140 and 180 hours, the rate of poisoning returns to the higher value. The amount accumulated in the HTD40 test is 1.2 %, which is greater than the 0.9 % accumulated in the LTD100 test. The middle core would be expected to accumulate the sum of the two, 2.1%, but has slightly less, 1.8 %. This could be because the substrate is saturated or because the location of the core has received less exposure to phosphorous. A paper by Benjamin et al. **[15]** shows that when a catalyst is supplied from an engine manifold under pulsating flow conditions the average flow can be lower in parts, notably at the centre, and greater around the periphery. A value of 1.8% for the mass of P in the crushed substrate segment, i.e. quarter core, is equivalent to 10.3 kg P / m^3. This is just above half of the value of 19.7 kg P/m^3 reactor used for C_{Winf} in Table 4.

Figure 8 shows the spatial profile along the samples for the LTD100 and the HTD40 experiments. More phosphorous accumulates in all four segments in the HTD40 experiment, where significant sintering is also occurring, than in the LTD100 case. It can be seen that in both tests phosphorous accumulates notably at the front end of the brick. The spatial concentration gradient from inlet to exit is flatter at higher flow rate under convective mass transfer conditions. As discussed above, the first segment of the middle core is seen to be capable of storing further phosphorous between 140 and 180 hours. The second segment of the middle core also achieves this although the third and fourth segments are similar in content to the HTD 40 samples. There is no suggestion in the shape of these profiles of a saturation condition being reached, although it is possible that the middle core front segment could be approaching saturation at 180 hours at its upstream end. The model discussed in this paper assumes that any phosphorous deposited contributes to the deactivation of the substrate.

There is the possibility, however, that some phosphorous deposited on the substrate does not deactivate the precious metal sites, but accumulates on an already deactivated site.

5.2 Predicted phosphorous build up and deactivation profiles

Finding the balance between poisoning and sintering that is required to obtain agreement between measurements and predictions of accumulated phosphorous in both the HTD40 and LTD100 cases is challenging.

Figure 9 shows predicted deactivation profiles and accumulated phosphorous from the combined model for the HTD40 case. The upper chart in Figure 9 shows the mass of P in each "disc". The 127 mm long core is imagined sliced into 64 discs of diameter 25.4 mm, so that each disc has length equal to the computational cell, just under 2mm. Phosphorous is predicted to accumulate at the front end of the core and continues to accumulate up to 40 hours. The lower figure shows that the model predicts that the catalyst activity is about halved at 8 hours and that further deactivation continues to 40 hours. Figure 10 shows a comparison between predicted amounts of accumulated phosphorous and measured values. The experimental results show that phosphorous continues to accumulate from 8 to 40 hours in the front segment. The model predicts steady accumulation of phosphorous over the 40 hour period with significant accumulation in the front segment. The data values might be expected to fall slightly below the predictions because the samples crushed for XRF analysis will have been subject to a small (< 2.5%) cutting loss. The total mass of P accumulated predicted by the model is approximately correct, but it was necessary to assume that half of the supplied phosphorous did not reach the substrate and was deposited in the engine or on the surfaces of the exhaust prior to the substrate in order to achieve this agreement. Significant brown staining from phosphorous compounds was observed in the supply pipework and on the ligament plate that supported the cores in the experiments **[16]**. The staining was greater in the LTD experiment than in the HTD experiment.

Figure 11 shows predicted deactivation profiles and accumulated phosphorous from the combined model for the LTD100 case. The figure also shows predictions of the deactivation experienced by the middle core, which includes additionally the HTD40 and HT40 tests giving 180 hours of ageing. The front of the catalyst is more deactivated than the rear. By 100 hours, activity is down to less than 1 % at the front but is still fairly high, about 80 %, at the rear. The accumulation of P has just reached saturation at 180 hours at the front end of the

core. The value 2.0E-05 kg/disc reached at the front end by 180 hours is equivalent to about 19.7 kg/m^3, which is the value used for C_{Winf}, see table 4. Figure 12 shows a comparison between predicted amounts of accumulated phosphorous and experimental measurements for both the LTD100 case and the middle core. The experimental results show that phosphorous continues to accumulate beyond 100 hours of ageing at all four segments. Comparison of the simulation with the experimental data in Figure 12 shows that the predicted amount of accumulated P at 100 hours agrees very approximately with the experimental data in all four segments. Agreement is also reasonable at 180 hours. Again, the data values might be expected to fall slightly below the predictions because the samples crushed for XRF analysis may have experienced a small cutting loss. Agreement has only been achieved by assuming that half of the poisoning dose was deposited prior to the substrate in the high temperature cases and three quarters in the low temperature case. The different mass flow rates, see Table 2, and the geometry of the engine and the supply pipework, see Figure 1, would clearly influence this.

Table 6 summarises the amounts of P supplied and stored in the two dosed experiments and simulations. The measurements and simulations suggest that for the LTD100 case almost all the phosphorous entering the brick is stored and that insignificant amounts pass out of the back of the brick. The shape of the simulation curve for the LTD100 case and the XRF data in Figure 12 show very small amounts of P stored in the fourth segment and this is consistent with minimal P slip by 100 hours. The HTD40 curve in Figure 10, on the other hand, shows significant P stored in the fourth segment at 40 hours and this condition will only be observed when some P passes through the brick without storage. The comparison of the simulation curve in Figure 10 with the XRF data at 40 hours, and the values in Table 6, suggest that the simulation may have under-estimated the slippage of P through the brick.

Figure 13 shows the predicted deactivation profiles for the HT40 case. The activity is reduced by more than 10% in the first hour but then is predicted to proceed to about 70% deactivation at 40 hours. Predicted deactivation is notably less in Figure 13 than in the combined HTD40 case, Figure 9. Figure 11 for the LTD case shows much more severe deactivation at the front than at the rear. This contrasts with Figure 13. The most severe deactivation of all the cases occurs in the middle core at 180 hours, see Figure 11, which is as would be expected.

6.0 Conclusions

The time dependency of accelerated test-bed ageing was measured by XRF chemical analysis on deactivated catalyst samples from an engine test bed experimental programme. Phosphorous was seen to build up at the front of the catalyst cores exposed to doped exhaust. Accumulation of phosphorous was still occurring at 100 hours in a low temperature dosed test and at 40 hours in a high temperature dosed test. The middle core was exposed to the 100 hours low temperature regime and 40 hours of high temperature sintering, and was still able to accumulate phosphorous when finally exposed to 40 hours of dosing at high temperature.

The model developed is able to predict deactivation from a combination of poisoning and sintering mechanisms. The amounts of accumulated phosphorous measured were compared against model predictions. The model was tuned by adjustment of the sintering constant. The model predicted P profiles that compared well with experimental observations. For both low and high temperatures agreement was good. The model was able to predict continuing deactivation throughout the ageing of the middle core. The amounts of P accumulated predicted for HTD40 and LTD100 were approximately correct but this was achieved by making an allowance for P deposited upstream of the test section.

Notation

A	sintering constant
A_{BET}	BET surface area per unit washcoat volume (cm^2/cm^3)
A_V	geometric surface area of monolith (m^2/m^3)
$C_{i\,g}$	mass fraction of species i in the gas phase
$C_{i\,sol}$	mass fraction of species i in the solid phase, i.e. in the pores of the washcoat
C_{Pg}	specific heat of gas (J/kg/K)
C_{Ps}	specific heat of substrate material (J/kg/K)
C_{SP}	molar concentration of poison precursor in washcoat pores (mol H_3PO_4/ cm^3)
C_{WP}	mass fraction of poison precursor in gas phase in washcoat pores (kg H_3PO_4/ kg air)
C_{Winf}	saturation concentration of phosphorous (kg P / m^3 reactor)
$C_{W\infty}$	saturation concentration of phosphorous (mol P / cm^2 BET)
d_h	hydraulic diameter of substrate channel (m)

D	active precious metal particle diameter during ageing (m)
D_O	initial precious metal particle diameter before ageing (m)
D_{WC}	diffusivity of H_3PO_4 in washcoat (m^2/s)
D_{air}	diffusivity of H_3PO_4 in air (m^2/s)
E	activation energy for hydrocarbon oxidation (J/mol)
h	heat transfer coefficient ($W/(m^2\ K)$)
H	nominal depth in washcoat (m)
K_{mi}	mass transfer coefficient of species i (m/s)
k_P	rate constant (originally, 0.1 cm/s)
K_P	rate constant [$\cong\ 0.000316\ \rho_g\ A_{BET}$] (m/s)
k_g	thermal conductivity of gas (W/(mK))
k_{sol}	thermal conductivity of substrate material (W/(mK))
M_i	molecular mass of species i (kg/mol)
$[\ O_2\ ]$	gas phase oxygen concentration, mass fraction
R	gas constant (J/mol/K)
R_i	reaction rate for species i ($mol/s/m^3$)
Sh	Sherwood number
T	temperature (K)
T_g	gas temperature (K)
T_{sol}	substrate temperature (K)
t	time (s)
Uc	velocity in the substrate channel (m/s)
U_S	superficial velocity in monolith, ε Uc (m/s)
V_w	fraction of monolith volume represented by gas in pores of washcoat
z	coordinate
ΔH	heat of reaction (J/mol)
ε	monolith porosity fraction
θ	fraction of catalyst sites free and active
θ_w	poisoned fraction of catalyst sites, poison coverage
ρ_g	density of exhaust gas (kg/m^3)

ρ_{sol} density of substrate material (kg/m^3)

Abbreviations

BET	Brunauer, Emmett and Teller surface area
CFD	Computational fluid dynamics
HTD	High temperature dosed
LTD	Low temperature dosed
HT	High temperature
XRF	X-ray fluorescence
ZDDP	Zinc dialkyldithiophosphate

Acknowledgements

W. Disdale was supported by an EPSRC case award in conjunction with the Ford Motor Company. The ageing of the catalyst cores took place at the Tickford Powertrain test facility, Banbury, UK.

References

[1] Zotin, F., Gomes, O., Oliveira, C., et al. Automotive catalyst deactivation: case studies. *Catalysis Today*, 2005, **107/108** , 157 – 167

[2] Chamberlain, W., Kelly, J., Wilk, M. The impact of passenger car motor oils on emissions performance. SAE Paper No. 2003-01-1988 (JSAE 20030347)

[3] Niura, Y., Ohkubo, K. Phosphorous compound effects on catalyst deterioration and remedies. SAE paper No. 852220 (1985)

[4] Gonzalez-Velasco, J., Botas, J., Ferret, R., et al. Thermal aging of Pd/Pt/Rh automotive catalysts under a cycled oxidizing-reducing environment. *Catalysis Today*, 2000, **59** , 395 – 402

[5] Nagashima, K., Nagata, M. Modeling of catalyst sintering and study of accelerated aging based on Pt/Al2O3 as a model catalyst. SAE Paper No. 2007-01-1134

[6] Oh, S., Cavendish, J.C. Design aspects of poison-resistant automobile monolithic catalysts. *Ind Eng Chem Prod Res Dev* , 1983, **22** , 509 – 518

[7] Matsunaga, S., Yokota, K., Hyodo, S., et al. Thermal deterioration mechanism of Pt/Rh three-way catalysts. SAE paper No. 982706 (1998)

[8] Baba, N., Yokota, K., Matsunaga, S., et al. Numerical simulation of deactivation process of three-way catalytic converters et al. SAE Paper No. 2000-01-0214

[9] Lassi, U. Deactivation correlation of Pd/Rh three-way catalysts designed for Euro IV emission limits. PhD thesis, University of Oulu, 2003

[10] Cooper, B. J., Evans, W. D. J., Harrison, B. Aspects of automotive catalyst preparation, performance and durability. Published in *Catalyst and Automotive Pollution Control*, Edited by A. Crucq and A. Frennet, Elsevier Science Publishers, Amsterdam, 1987

[11] Benjamin, S. F., Roberts, C.A. Automotive warm up to light-off by pulsating engine exhaust. *Int J Eng Res*, 2004, **5**,125 – 147

[12] Benjamin, S. F., Roberts, C. A. Three dimensional modelling of NOx and particulate traps using CFD: A porous medium approach. *Applied Mathematical Modelling*, 2007, **31**, 2446 - 2460

[13] Gueveremont, J. M., Guinther, G., Jao, T-C., et al. Total phosphorous detection and mapping in catalytic converters. SAE paper No. 2007-01-4078

[14] Shah, R. K., London, A. L. Laminar flow forced convection in ducts. Academic Press Inc, 1978.

[15] Benjamin, S., Disdale, W., Liu., Z. et al. Velocity predictions from a coupled 1D/3D CFD simulation compared with measurements in the catalyst system of a firing engine. *Int J Eng Res*, 2006, **7** , 29 - 40

[16] Disdale, W. An experimental and computational investigation of the time dependency of automotive catalyst deactivation. PhD Thesis, Coventry University, UK, 2007

Table 1 Details of the catalyst core ageing regimes

Order	Ageing Regime	Code	Temperature K	ZDDP in fuel ppm	Engine Condit.	Ageing hours	Core change hours
1	**Low temperature dosed**	LTD	818	150	2000 rpm 20 – 30 Nm	100	20
2	**High temperature**	HT	1118	0	4500 rpm 70 – 80 Nm	40	8
3	**High temperature dosed**	HTD	1118	90	4500 rpm 70 – 80 Nm	40	8

Table 2 Mass flow rates and concentrations of poison precursor

Ageing regime	Total mass flow to 7 cores, kg/s	P mass fraction	H_3PO_4 mass fraction	Total mass of P supplied to 7 cores, kg
LTD100	0.00904	8.71E-07	2.755E-06	0.00283
HT40	0.042	–	–	-
HTD40	0.042	5.23E-07	1.654E-06	0.00317

Table 3 Details of catalyst cores analysed

.

Ageing Regime	Hours aged	Position in core holder
HTD	8	1
	16	2
	24	3
	32	4
	40	5
	40	TC
LTD	20	1
	60	3
	100	5
	100	TC
HT	8	1
	24	3
	40	5
All regimes	180	M
Control	0	Fresh Core

Table 4 **Parameter values used in the deactivation model**

Parameter	Value	Units
A	1.5E−15	
C_{WP} (LTD100 case) - phosphorous	8.71E−07	kg P / kg air
C_{WP} (LTD100 case) - precursor	2.755E−06	kg H_3PO_4 / kg air
C_{WP} (HTD40 case) - phosphorous	5.23E−07	kg P / kg air
C_{WP} (HTD40 case) - precursor	1.654E−06	kg H_3PO_4 / kg air
Factor applied to Cwp (LTD100)	0.25	
Factor applied to Cwp (HTD40)	0.5	
T (LTD 100 case)	818.0	K
T (HT40 and HTD40 cases)	1118.0	K
Rate constant, Kp	0.000316 ρ_g A_{BET}	m/s
A_{BET}	17.4E+06	m^2/m^3
C_{Winf}	19.7	kg P / m^3 reactor
[O_2] mass fraction	0.00387	
E/R for hydrocarbon oxidation	−15562.0	K
D_O	5.0E−10	m

Table 5 **Time step scheme for 180 hours middle core ageing simulation**

Load step	No. of time steps	Time step (s)	Total time	Courant No.
1	3000	0.02	60 secs	< 50
2	2400	0.1	4 minutes	–
3	660	5.0	55 minutes	–
4	2970	120	99 hours	–
5	1200	120	40 hours	–
6	1200	120	40 hours	–

Table 6 **Total mass of P deposited in cores in experiments and simulations**

Ageing regime	Total mass of P supplied in expt., g	Mass of P supplied per core in expt., grams	Factor from Table 4	Mass of P input to simulation, g	Mass of P stored in simulation, g	Mass of P measured by XRF, g
LTD100	2.83	0.404	0.25	0.101	0.100	0.108
HTD40	3.17	0.453	0.5	0.226	0.204	0.198

List of captions for the illustrations

Figure 1

Photograph of engine test rig showing demountable catalyst core holder, circled.

Figure 2

Dimensions of the catalyst core holder.

Figure 3

Core numbering scheme for catalyst core samples.

Figure 4

Analytical predictions of active surface area at the catalyst inlet using estimated pore phase concentrations of poison precursor and oxygen: LTD100 case (mainly poisoning), HT40 case (sintering only) and HTD40 case (both poisoning and sintering).

Figure 5

Mesh with fluid and solid cell blocks for full ageing simulations, i.e. combined poisoning and sintering, on 127 mm length core samples.

Figure 6

Results from XRF analysis showing the elements found in the inlet segment of cores.

Figure 7

Accumulated phosphorous in first segment of core as a function of time. Middle core experiences no poisoning during HT40 regime between 100 and 140 hours.

Figure 8

Poison profiles for phosphorous at the end of tests found by XRF analysis.

Figure 9

Simulation of HTD40 case. The hypothetical disc is a slice of core with diameter 25.4 mm and length equal to the length of the computational cell.

Figure 10

XRF data compared with simulation for the HTD40 case.

Figure 11

Simulation of LTD100 case and the middle core. The hypothetical disc is a slice of core with diameter 25.4 mm and length equal to the length of the computational cell.

Figure 12

XRF data compared with simulation for the LTD100 case and the middle core.

Figure 13

Simulation of change in active fraction, theta, with time for the HT40 case, sintering at 1118K.

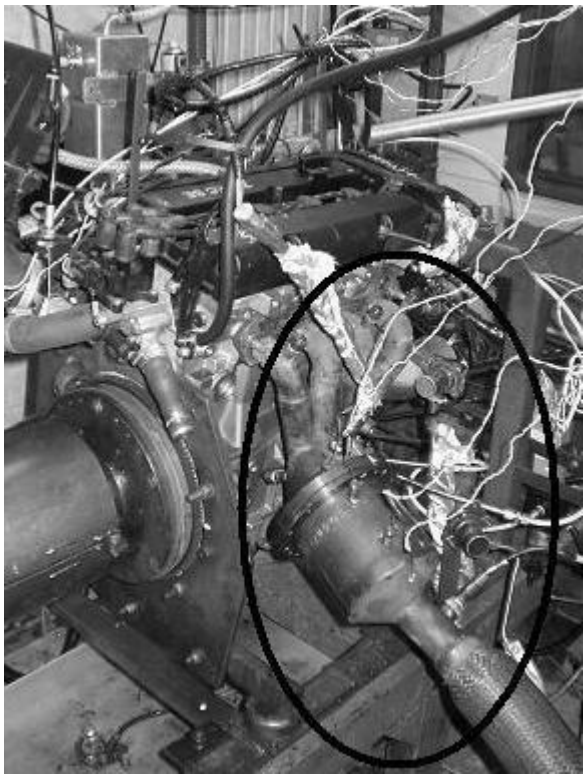

Fig. 1 *Photograph of engine test rig showing demountable catalyst core holder, circled.*

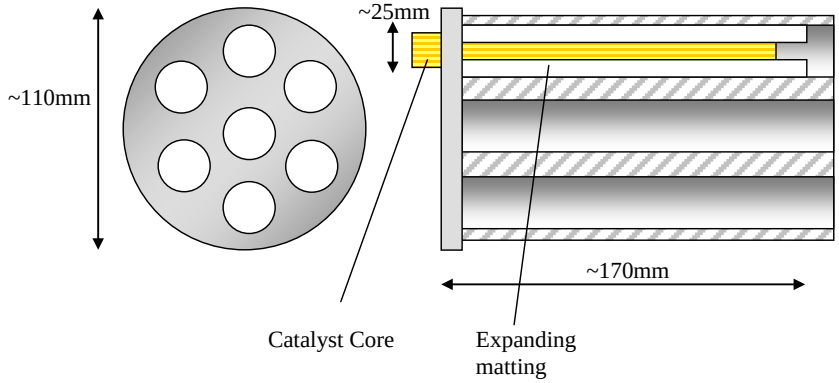

Fig. 2 *Dimensions of the catalyst core holder.*

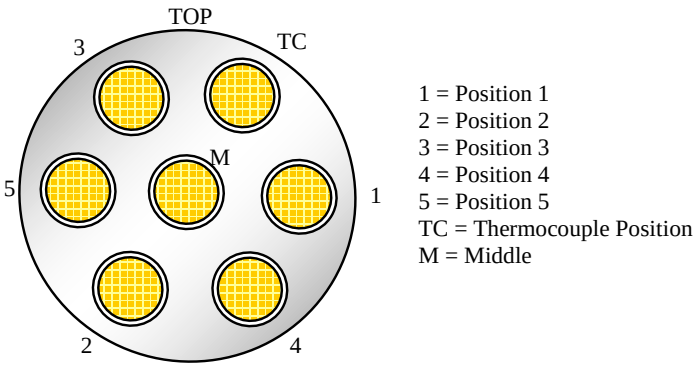

Fig. 3 *Core numbering scheme for catalyst core samples.*

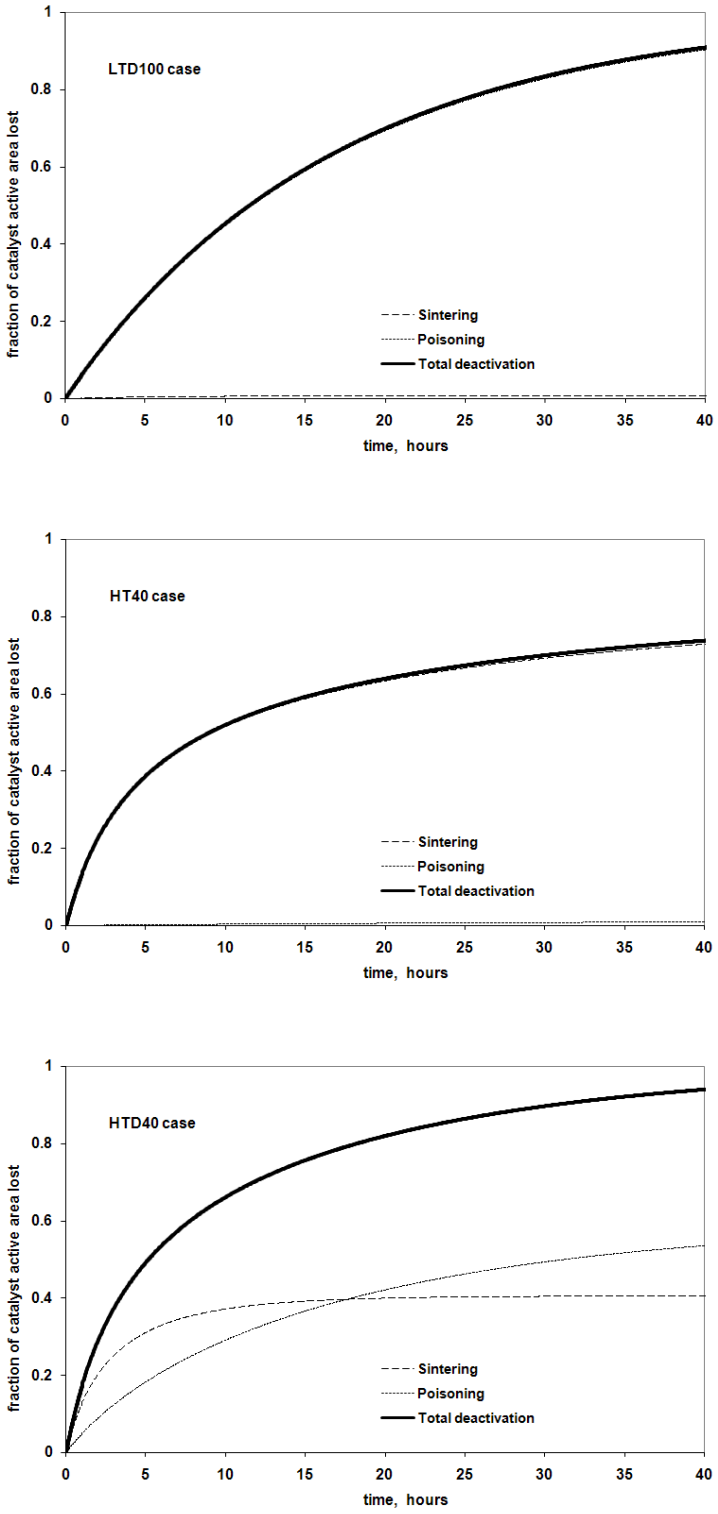

Fig. 4 *Analytical predictions of active surface area at the catalyst inlet using estimated pore phase concentrations of poison precursor and oxygen: LTD100 case (mainly poisoning), HT40 case (sintering only) and HTD40 case (both poisoning and sintering).*

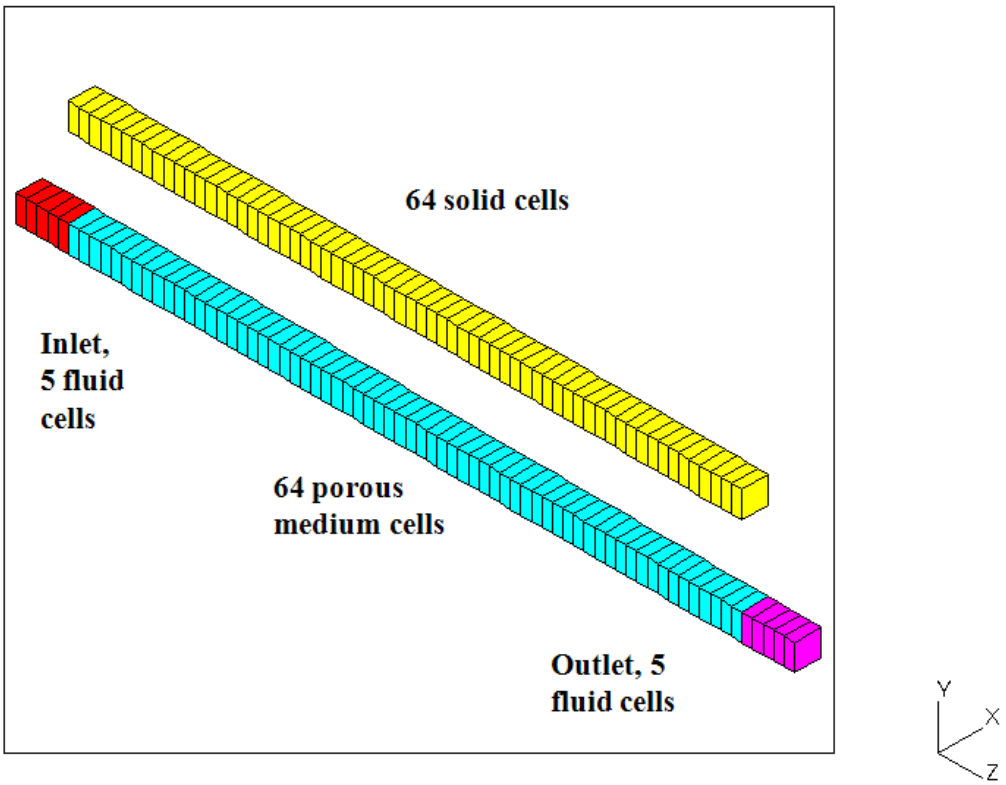

Fig. 5 *Mesh with fluid and solid cell blocks for full ageing simulations, i.e. combined poisoning and sintering, on 127 mm length core samples.*

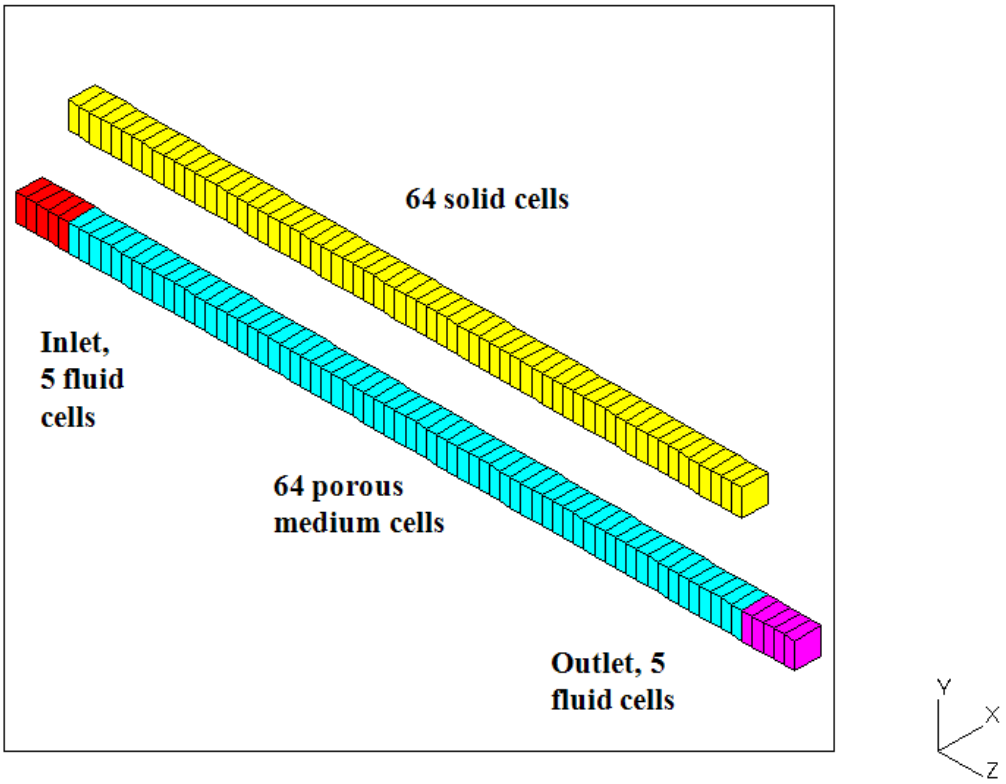

Fig. 5 *Mesh with fluid and solid cell blocks for full ageing simulations, i.e. combined poisoning and sintering, on 127 mm length core samples.*

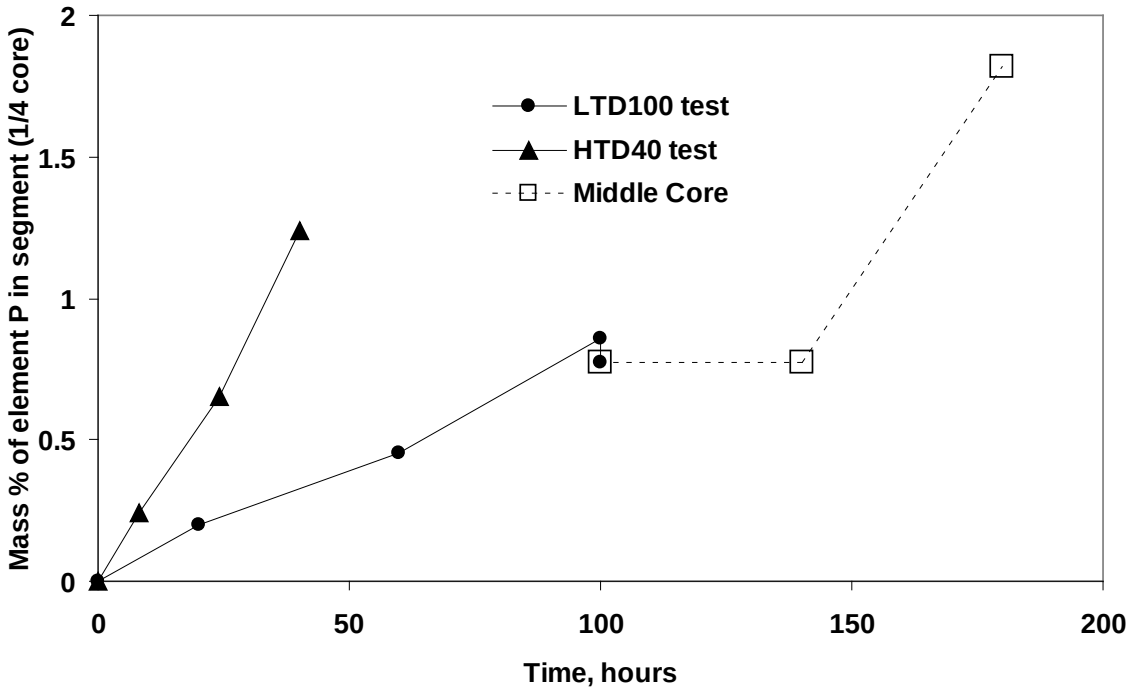

Fig. 7 *Accumulated phosphorous in first segment of core as a function of time. Middle core experiences no poisoning during HT40 regime between 100 and 140 hours.*

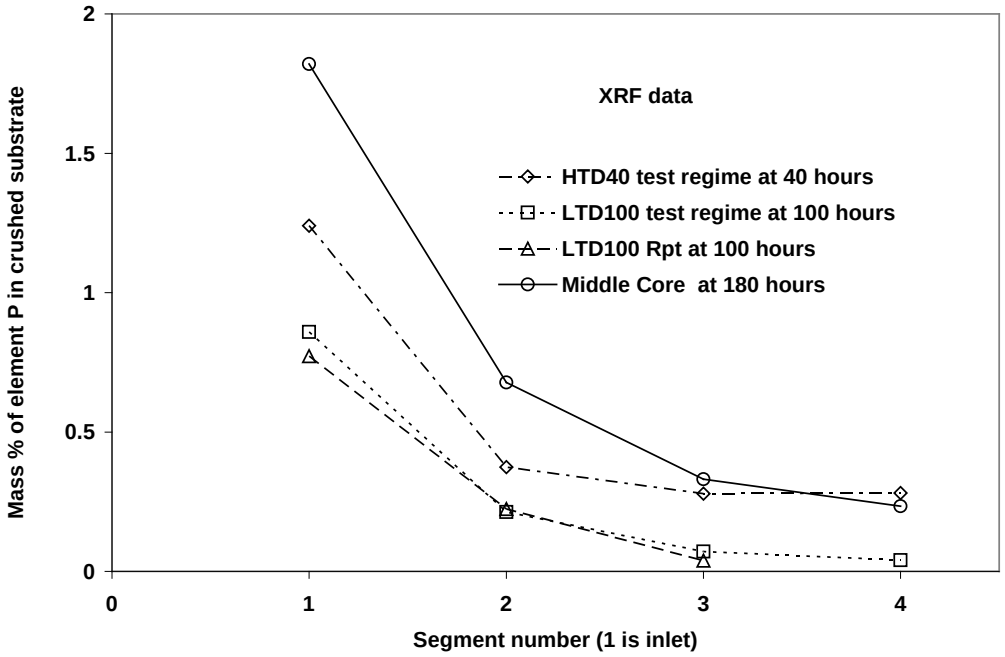

Fig. 8 *Poison profiles for phosphorous at the end of tests found by XRF analysis.*

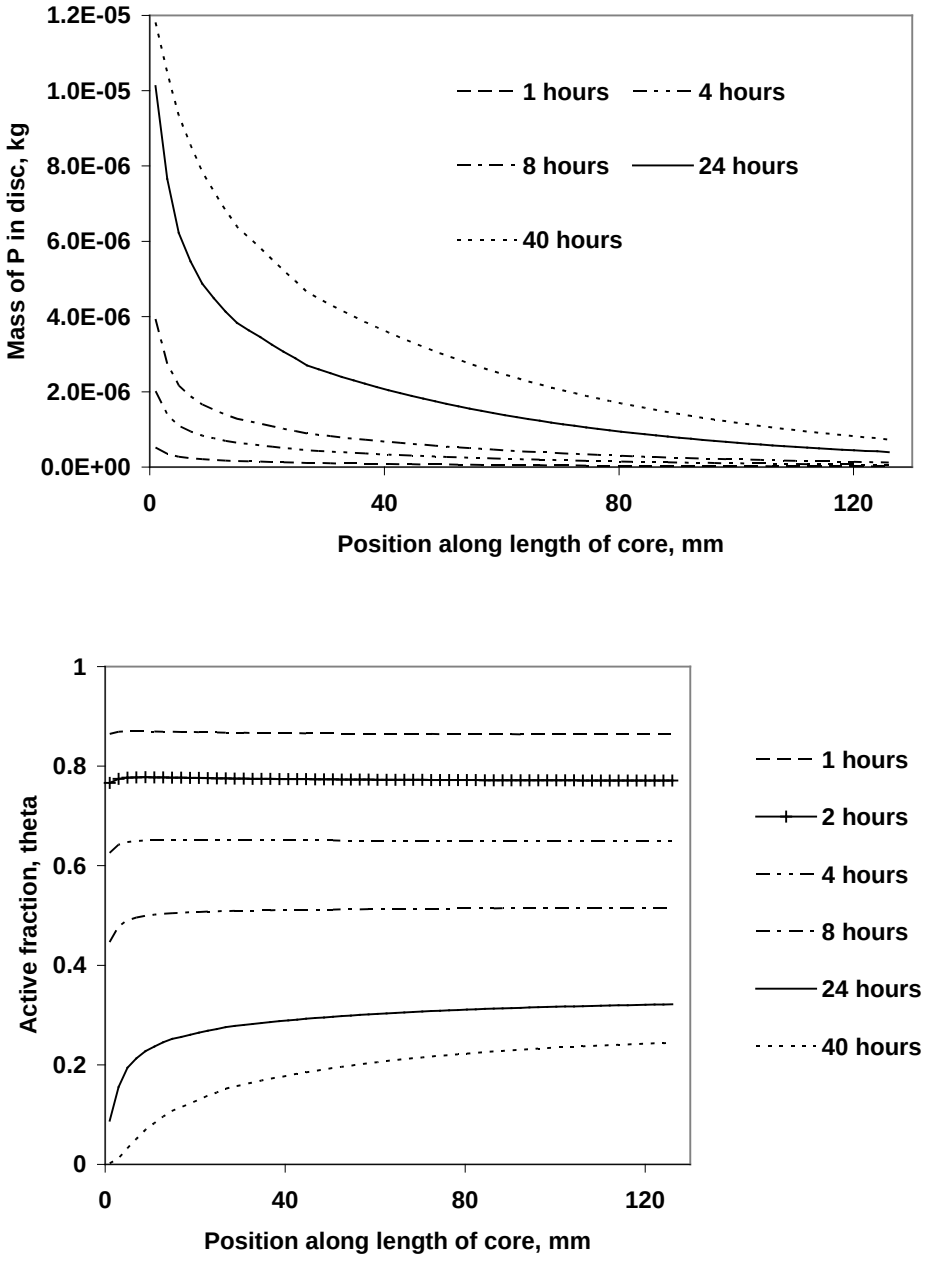

Fig. 9 *Simulation of HTD40 case. The hypothetical disc is a slice of core with diameter 25.4 mm and length equal to the length of the computational cell.*

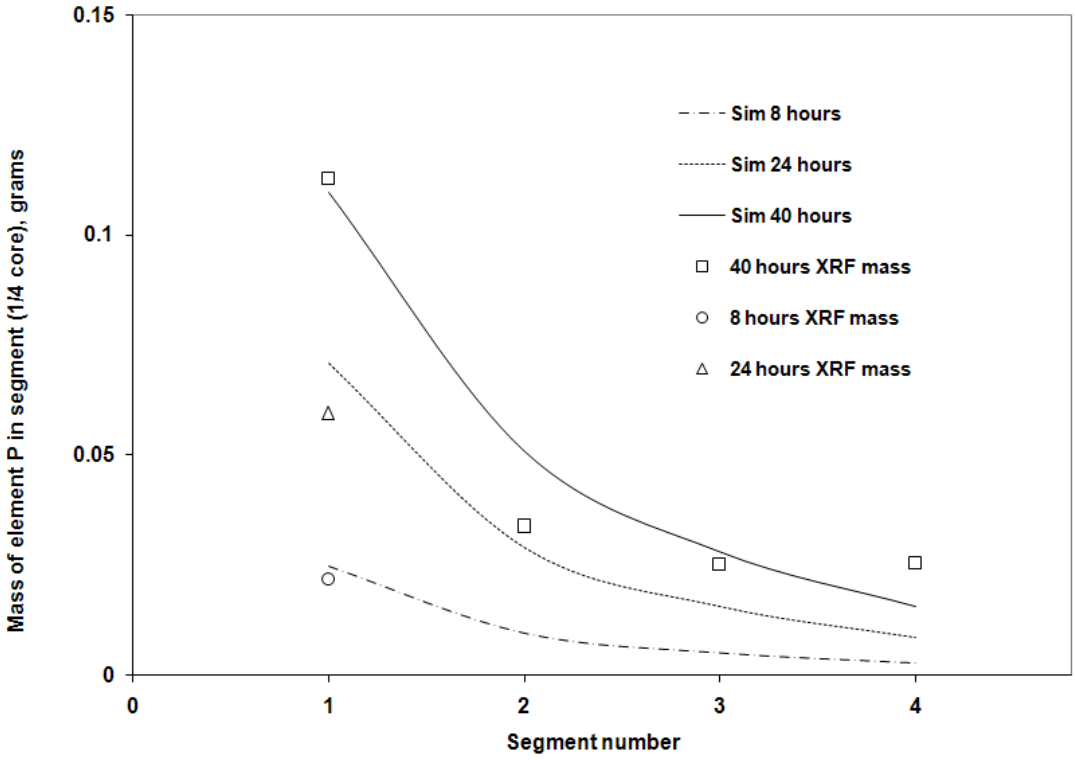

Fig. 10 *XRF data compared with simulation for the HTD40 case.*

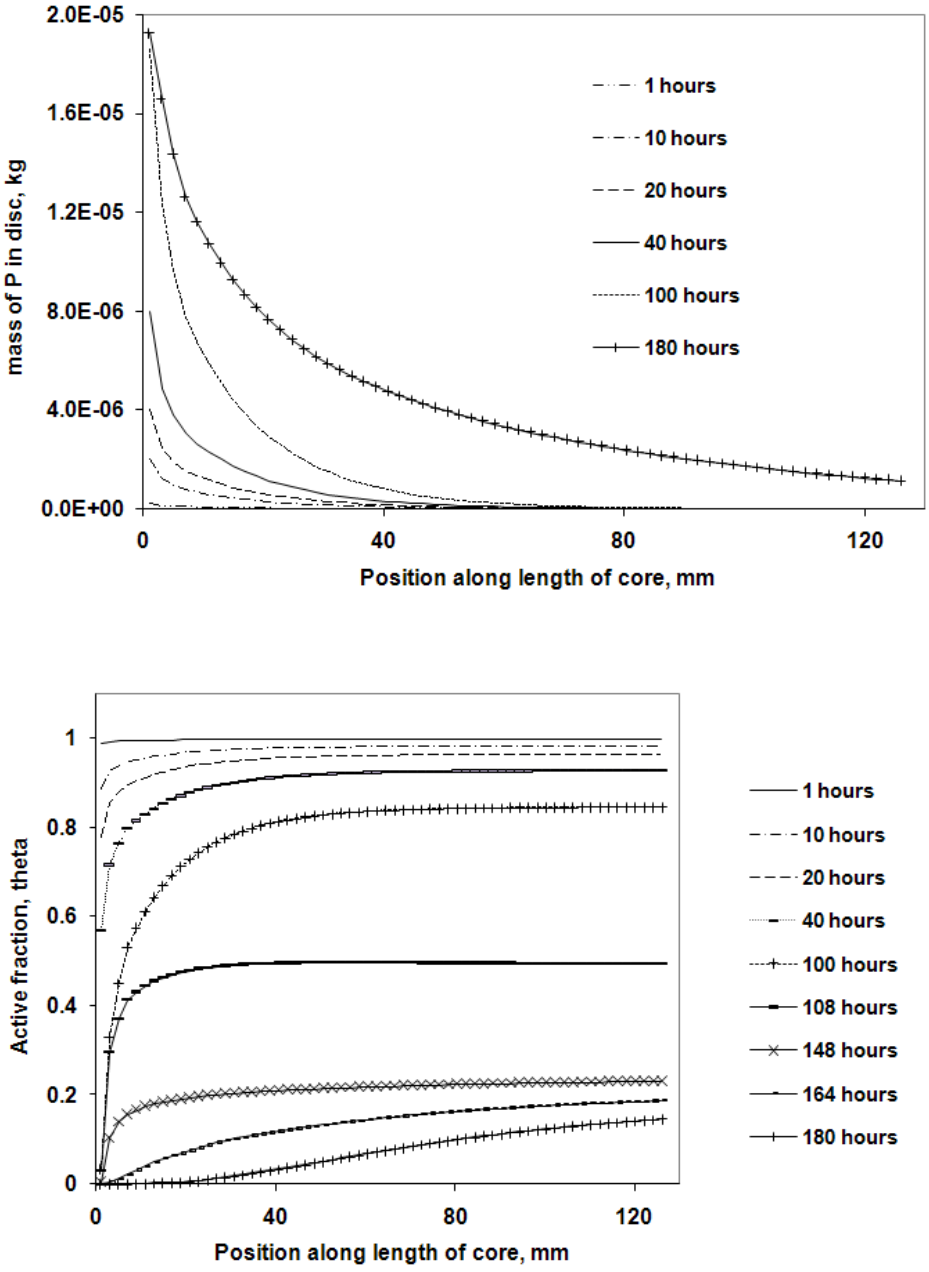

Fig. 11 *Simulation of LTD100 case and the middle core. The hypothetical disc is a slice of core with diameter 25.4 mm and length equal to the length of the computational cell.*

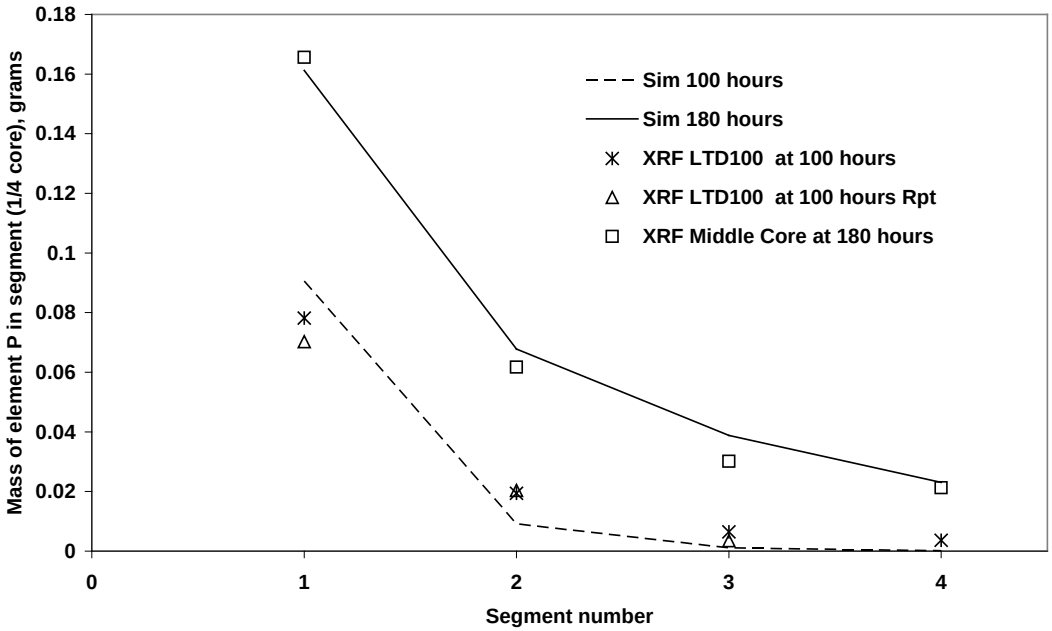

Fig. 12 *XRF data compared with simulation for the LTD100 case and the middle core.*

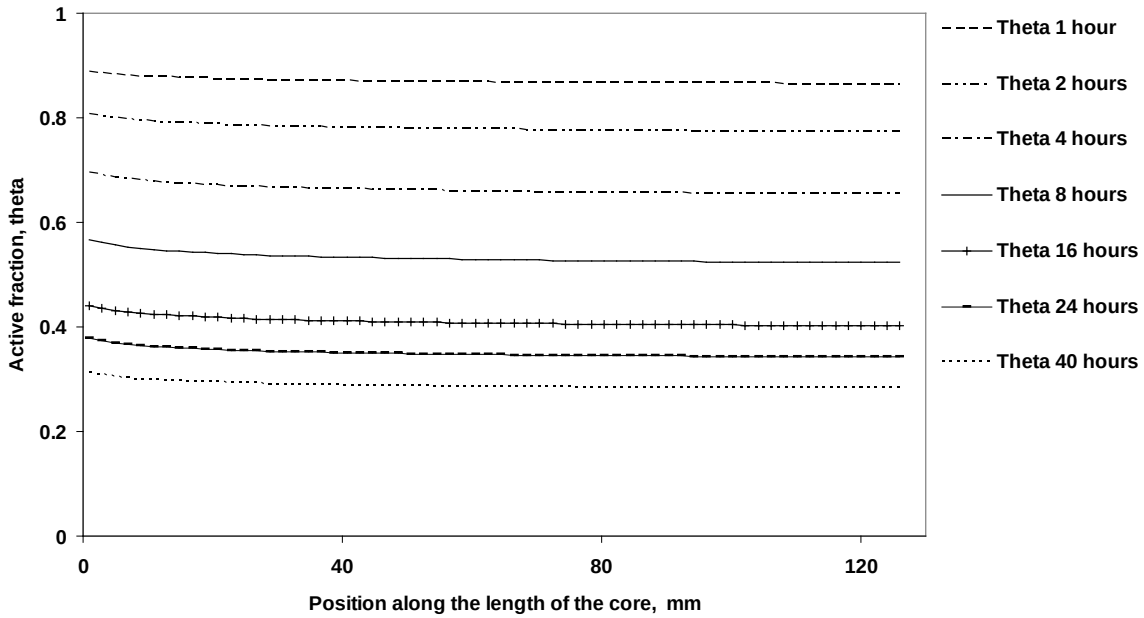

Fig. 13 *Simulation of change in active fraction, theta, with time for the HT40 case, sintering at 1118K.*